ISSN 1996-3343

Asian Journal of Applied Sciences

http://knowledgiascientific.com

Knowledgia SCIENTIFIC
A Place to Publish Outstanding Research

Asian Journal of Applied Sciences 2 (3): 253-274, 2009
ISSN 1996-3343

A Novel and Proven System for Non-Invasive Blood Glucose Monitoring using HbA1C

[1]J. Sundararajan, [2]V. Palanisamy and [1]Mandyam Sandeep
[1]Paavai Engineering College, NH-7, Pachal, Namakkal-637 018, India
[2]Info Institute of Engineering, Coimbatore-641107
Tamil Nadu, India

Abstract: In this study, we present a novel framework for blood glucose level measurement using a combination of the HbA1c test and the stable, accurate Photo Acoustic methods to get an absolutely consistent and precise, non-invasive technique. The setup uses a pulsed laser diode as a source rather than the typical Nd: YAG laser, since it gives a possibility for variable input wavelength pulses. The detector has a double ring sensor as the main module. It is based on the piezoelectric detection. The two ring sensor is used since it has a small opening angle. The detector setup used in this application consists of a ring detector that includes two double ring sensors that are attached to the ring shaped module that can be worn around the finger. The major aim is to detect the photo acoustic signals from the glycated hemoglobin with the least possible error. The proposed monitoring system is designed with extreme consideration to the precision and the compatibility with the other computing devices. The results obtained in this research have been studied and analyzed by comparing these with the results with the *in vitro* techniques like the HPLC. The comparison between the two results has been plotted and it shows a least error. The results also show a positive drive for using this concept as a basis for future extension in quantifying the other blood components.

Key words: Photo acoustic (PA), HbA1C, pulsed repetition frequency, pulsed laser diode, double ring senor, direction sensitivity

INTRODUCTION

Diabetes is presently considered one of the most bothersome diseases due to the complications involved in its treatment and due to the other complexities that it leads to. The complications resulting from the diseases are a significant cause of morbidity and mortality and are associated with failure of various organs such as the eyes, kidneys and nerves. Diabetics are also at a significantly higher risk for coronary artery disease, peripheral vascular disease and stroke and they have a greater likelihood of having hypertension dyslipidemia and obesity. Diabetes exists not as an independent disease but leads to a number of problems. Diabetes is not of one type. There are three main types of diabetes:

- Juvenile-onset (type 1) or insulin-dependant diabetes mellitus (IDDM)
- Adult-onset (type 2) or non-insulin dependant diabetes (NIDDM)
- Gestational diabetes

These three conditions mentioned account for over 98% of all diabetes. It has been estimated that Non-Insulin Dependent Diabetes Mellitus (NIDDM) is the most rapidly growing chronic metabolic

Corresponding Author: J. Sundararajan, Department of ECE, Paavai Engineering College, Salem-Namakkal Highways (NH-), Pachal, Namakal (Dt.), Tamil Nadu-637018, India

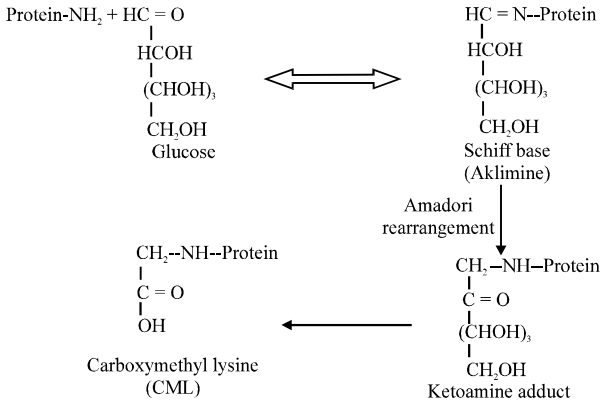

Fig. 1: Amadori rearrangement

disorder in the world. The measurement of the total glycated hemoglobin concentration is the widely used blood test for quantifying glucose in normal as well as diabetic patients. The reason for this is the versatile nature of this molecule. The complications associated with diabetes are mainly due to the non-enzymatic glycation of proteins (Brownlee, 2000; McCance *et al*., 1993; Thorpe and Baynes, 1996; Vlassara *et al*., 1986). The Maillard hypothesis suggests that chemical modification of proteins by glucose and subsequent reactions of the adduct may result in products which are directly responsible for many pathological conditions in diabetes (Brownlee, 2000; Brownlee *et al*., 1988; Vlassara *et al*., 1992). The reaction of glucose with amino groups in proteins results in the reversible formation of a Schiff's base or aldimine, which can undergo irreversible Amadori rearrangement (Fig. 1) to form a ketoamine product. Glycation is also a process that appears to be associated with age-related disorders and may be particularly important in the context of long-lived proteins which do not undergo rapid synthesis and turnover (Thorpe, 1996; Jean-Lue Wautier and Guillausseau, 1998).

The purpose of many such studies was the characterization of site-specificity of glycation and the factors catalyzing rearrangement to the Amadori product. At present, the technique for quantifying HbA1C (glycated hemoglobin) concentration is invasive and cannot provide results rapidly. Here we propose to use a photo acoustic technique for non-invasive and accurate measurement of HbA1C concentration.

The photo acoustic technique is based on the generation of a near infrared wave by pulsed laser diode and time-resolved detection of the acoustical wave by the acoustical transducer. It can be used for tissue characterization with high contrast (photo acoustic signal parameters are dependent on the optical properties of the irradiated tissue) and high resolution due to time-resolved detection of acoustic waves. Since hemoglobin A1C (HbA1C) is the post transnational modification of glucose and hemoglobin, the major blood component, the photo acoustic technique is sensitive to variation of its concentration.

The variation of HbA1C concentration in blood and its behavior under photo acoustic signals, the blood vessel diameter and photo acoustical transducer displacements on signals recorded in transmission and reflection models from a phantom of the radial artery were studied. The outputs of this method were compared with those of the standard *in vitro* techniques and they showed a very good acceptability range.

The glucose molecules in the blood attach themselves to many of the chemical compounds like hemoglobin, Low Density Lipoprotein (LDL's), serum proteins (like albumin) and many more. When it is in the free aldehyde form, it can react with the hemoglobin molecule within the red cells of blood to form an aldimine adduct as shown in the Fig. 1. But this is a reversible reaction in equilibrium with

the blood glucose and hence this aldimine adduct is labile. However it can undergo a shift in the double bond to the second carbon in an Amadori Rearrangement (Seetharama Acharya and Manning, 1980) to form a ketoamine adduct as shown. This ketoamine adduct is an irreversible arrangement of the hemoglobin and glucose molecules.

The changes in the chemical bonds, particularly the double bonds involving the first and second carbon of glucose modify both the electronic transition and molecular vibration environments from those of free glucose and hemoglobin to those of the adducts. Therefore, the optical absorption spectra and the photo acoustic spectra of the free glucose and hemoglobin, the aldimine and the ketoamine are each sufficiently different to form the basis for spectroscopic determination of the amounts of each form present in the blood. Now HbA1C is the most prevalent of the ketoamine adducts with the β chain of the hemoglobin, representing 5-6% of the total hemoglobin in persons without diabetics. This gives the justification for the choice of HbA1C for glucose quantification.

Having identified the difficulties with the diabetic patients in measuring their blood glucose levels, research has led to a number of blood glucose quantification techniques. Apart from the individual demerits, the invasive methods (Shults *et al*., 1994; Sternberg *et al*., 1995) have a common drawback that they cause pain and inconvenience to the patient. In view of the fact that the main aim of the *in vivo* technique is to create a patient-friendly system, the invasive systems can well be crossed out.

Arriving at the non-invasive and minimally invasive methods of glucose level measurement there are a lot of techniques in the developmental phase and research is extensively being done in this area. Some of these existing techniques are described briefly.

NIR spectroscopy (Fischbacher *et al*., 1997) has been a regular choice for the study of the glucose measurement. But the main difficulties with this technique are the large absorption values of water and the similar absorption behavior of proteins and non-glucose metabolites. The key problem is that the spectral variations due to glucose concentration are extremely small compared to that from other biological components. In addition, there are also some ambiguous time-dependent physiological processes, which make the explanation of the model more difficult, especially in the universal calibration.

Near Infrared Diffuse-Reflectance Spectroscopy is also a popular field of research which utilizes the reflectance properties of NIR. The problem of light scattering, diffusion (Ishimaru, 1989; Edward Profio, 1989) and absorbance interferes with this technique causing errors and another drawback is that separate calibration models should be used for each person in the tests. Thermal infrared vibrational spectroscopy is based on the principle that vibrational motions occur within a crystal lattice at fundamental frequencies that are directly related to the crystal structure and elemental composition (Wilson *et al*., 1955; Griffiths, 1972; Lane and Christensen, 1997). The device setup in this technique has demonstrated only a reasonable accuracy of measurement in glucose with the mean absolute relative error at 11.6% for which alternate techniques can be preferred.

Raman spectroscopy (Dou *et al*., 1996) offers the possibility of remotely obtaining a measurement of glucose *in vivo* because, in contrast to infrared spectroscopy, its spectral signature is not obscured by water. In addition, Raman spectral bands are considerably narrower than those produced in classical infrared spectral experiments and Raman excitation in the near infrared region (700-1300 nm) encounters minimal fluorescence in aqueous media. It is relatively inexpensive, but there is a problem with noise in the signal and it is currently under developmental phase.

The HbA1C test is briefly explained here. The percentage of glycated hemoglobin in the blood and its interpretation in terms of glucose levels is given in the Table 1. One important goal of diabetes treatment is to keep the blood glucose levels near the normal range of 0.7-1.2 kg L^{-1} before meals and under 1.4 kg L^{-1} at 2 h after eating. Since blood glucose levels can fluctuate widely, even frequent home glucose testing may not accurately reflect the degree of success in controlling blood sugar. The HbA1C test is a valuable measure of the overall effectiveness of blood glucose control over a period of time.

Table 1: Relationship of A1C to average whole blood and plasma glucose levels

Interpretation	Average plasma glucose	Mean blood glucose (mg dL^{-1})	HbA1C (%)
Non-diabetic range	65	61	4
	100	92	5
	135	124	6
Target for diabetes in control	170	156	7
Action suggested according	205	188	8
ADA guidelines	240	219	9
	275	251	10
	310	283	11
	345	314	12

In individuals with poorly controlled diabetes, increases in the quantities of these glycated hemoglobins are noted. The HbA1C level is proportional to average blood glucose concentration over the previous four weeks to three months. The glycated hemoglobin test gives accurate glucose measurements to maximum extent since the concentration of glucose in the blood is proportional to the extent of glycosylization of the hemoglobin. In most labs, the normal range is 4-5.9%. In poorly controlled diabetes, its 8.0% or above and in well controlled patients it's less than 7.0%. The benefits of measuring HbA1C is that is gives a more reasonable view of what's happening over the course of time (3 months) and the value does not bounce as much as finger stick blood sugar measurements. The percentage of glycated hemoglobin in the blood and its interpretation in terms of glucose levels is given in the Table 1. But the disadvantage of the HbA1C test is that the normal values for the glycated hemoglobin test may vary from laboratory to laboratory because different laboratories use different procedures to perform the measurement. As a result of this diabetics may be restricted to taking their test only from a particular lab affecting their professional schedules or the diabetics may have to include their medical reports along with the documentary and carry it around, everywhere.

MATERIALS AND METHODS

Methods and Designs

As mentioned, a combination of photo acoustic methods and the HbA1C test has been used here. Photo acoustics has many applications (Freeborn *et al*., 1998; Petrova *et al*., 2004) and bio medical engineering is one particular area that has taken photo acoustics into deep consideration. The following sections describe the methods and the designs involved in this study. It gives the photo acoustic analysis and the technical details of all aspects of this study.

Generation of Photo Acoustic Waves

Photo Acoustic waves can be generated when modulated energy beams, such as those comprised of electromagnetic radiation, x-rays, electrons, protons, ions and other particles, interact with matter. The various mechanisms capable of generating PA waves are shown in Fig. 2.

But among all the above mentioned sources, the modulated light energy is used in this paper to generate PA waves. This is because light consists of non-ionizing radiation, which is not harmful to the human body and there are abundant, economical and effective optical sources and devices. The chief principle that is used in the PA mechanism is the optical absorption followed by thermal de-excitation. The basis for using thermal expansion from among various other mechanisms in the glucose quantification is that it does not break or change the properties of the object under study. It also has a linear or a definite relationship with many of the physical parameters of diverse materials and it is non-destructive or non-invasive in application such as materials test and medial diagnosis.

Thermal Expansion

The in progress technique would employ high peak power pulsed laser diodes which are compact, relatively inexpensive and available in a wide variety of NIR wavelengths in preference to the

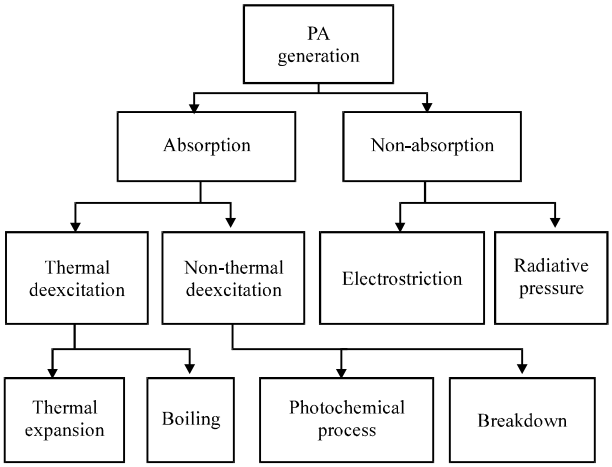

Fig. 2: Different PA generating mechanisms

Q- switched Nd: YAG lasers which are bulky and expensive with limited scope for varying the pulse repetition frequency, wavelength and pulse width as excitation sources. When the light from these laser diodes irradiates the skin and tissues (absorbing medium), the ion specific absorption in the illuminated region produces heat due to non-radiative relaxation. This heat causes the region to expand. If the pulse duration of the laser is short enough or its modulated frequency rapid enough, the thermal expansion will be exceedingly fast. Due to this action, an acoustic wave is generated and propagated outside. This wave is subsequently detected by an acoustic transducer. The amplitude of the acoustic wave is linearly proportional to the absorbed energy density, while the shape of the wave is dependent on the absorption distribution, laser parameters and boundary condition.

Direct and Pulsed Mode PA Technique

From the direct and indirect methods of PA technique, the direct method in which a portion of an incident light will penetrate into the sample and generate an acoustic wave within it (provided that the optical absorption of a sample is not too high) is opted for owing to some of its advantages. It's most important benefit is that the sample does not need to be enclosed in a volume, which is an important consideration for the *in vivo* determination and imaging of the glucose concentration. Among from the continuous wave and pulsed mode PA techniques, the pulsed mode scheme is selected. This is because in continuous wave mode the duty cycle of the modulated beam is close to 50% due to which it may produce spurious effects, such as heating of the sample and convection currents. Furthermore, the CW mode suffers from apparent thermal diffusion in the generation of the PA response, thereby lowering its PA efficiency and sensitivity. In addition, the CW mode is inapplicable to biomedical PA imaging and diagnosis.

Hence the thermal elastic direct PA generation by pulsed excitation mode will be the PA technique used in the *in vivo* technique that is being discussed.

Excitation System-High-Peak Power Pulsed Laser Diodes

For an effective generation of PA signals, laser pulse durations in the range of tens to hundreds of nanoseconds are required. Also to acquire sufficient penetration depth, the near infrared (NIR) range (600-1200 nm) should be used as at such a wavelength the biological tissues are pretty translucent. The Q-switched Nd: YAG laser operating at 1064 nm can satisfy the above demands. But it can provide only a fixed NIR wavelength which restricts its use in the quantification and analysis of some blood

components like oxy-hemoglobin and deoxy-hemoglobin. Despite the fact that the main goal of the paper is glucose quantification for which the Nd: YAG laser excitation system can be used, we opt for the pulsed laser diode system since our core principle can be well extended to quantify other blood components in future study. The high peak power pulsed laser diode system is used in preference than the typical Q-switched Nd: YAG laser because apart from providing only a single fixed NIR wavelength, it is also bulky with large cooling requirements. Comparatively the pulsed laser diode system is economical with simpler driver electronics apart from giving a wide range of NIR wavelengths. Another reason why the laser diodes are preferred is that the Pulse Repetition Frequencies (PRF's) of the Nd: YAG laser excitation system is of the order of few tens of hertz while that of the pulsed laser diode is of the order of few kHz. But the primary disadvantage of the laser diode is its low peak output power which is typically less than around 200 Watts. The pulse energies obtained for nanosecond duration in an Nd: YAG laser is of the order of milli joules while that of a pulsed laser diode is of the order of micro joules. This limitation can be alleviated. Thomas *et al*. (2006) has developed a single-wavelength system to demonstrate that PA signals of adequate SNR can be generated. Their under lying concept was that since the PRF of a pulsed laser diode can be of the order of kilohertz compared to a few tens of hertz for Q-switched-based excitation systems, with a suitably fast acquisition system this would allow several thousand PA signals to be acquired and the signal can be averaged in a fraction of a second, increasing the Signal-to-Noise Ratio (SNR).

Effect of Pulse Duration on the Photo Acoustic Signal

The two models that are used to simulate the effect of pulse duration on the photo acoustic signal are the analytical and numerical models. The two of them are briefly described here.

Analytical Model

By Lambert-Bouguer law, when collimated light is incident on a pure absorber its intensity will decrease exponentially due to the absorption of the medium.

$$I(z) = I_0 \exp(-\mu_a z)$$

where, I (z) is the intensity at depth z, I_0 is the intensity at the surface and μ_a is the absorption coefficient of the pure absorber. The absorbed light will create a temperature rise in the medium causing it to expand. This increase in volume is proportional to the change in temperature θ and can be expressed by:

$$\Delta V = \beta \theta V$$

where, β is the thermal expansion coefficient of the medium and v the initial volume of the heated region. The expansion will cause strain in the heated volume, consequently generating stress which will excite pressure waves. The initial pressure P_o is:

$$P_o = B(\Delta V/V)$$

where, B is the isothermal bulk modulus. From the above two equations we get:

$$\beta \theta V = (P_o V)/B \rightarrow P_o = B\beta\theta$$

Thus we can get the pressure P_o as a function of the temperature θ.

Numerical Model

The reason for a numerical model is that the analytical expression for the photo acoustic signal was developed for an impulse and a rectangular pulse of finite duration and since this assumes a photo acoustic source of infinite lateral extent, it is problematic to validate experimentally. This numerical model can simulate photo acoustic signals emitted by a source of finite lateral dimensions. The experimental validation of the numerical method has also been proved in the reference.

THE DETECTOR DESIGN

Piezoelectric Constants

A piezoelectric ceramic is anisotropic and hence the physical constants relate to both the direction of the applied mechanical or electric force and the directions perpendicular to the applied force. Consequently, each constant generally has two subscripts that indicate the directions of the two related quantities, such as stress (force on the ceramic element/surface area of the element) and strain (change in length of element/original length of element) for elasticity (Fig. 3).

The direction of positive polarization usually is made to coincide with the Z-axis of a rectangular system of X, Y and Z-axes. Direction X, Y, or Z is represented by the subscript 1, 2, or 3, respectively and shear about one of these axes is represented by the subscript 4, 5, or 6, respectively. The piezoelectric charge constant, d, the piezoelectric voltage constant, g and the permittivity, e, are temperature dependent factors (Diebold, 1994).

Photo Acoustic Wave Detection

Thin piezoelectric sensors (Jackson, 1980) make use of a piezoelectric element, which thickness t_p is much smaller than the lateral dimensions. Here, the piezoelectric voltage as a function of time, generated by a photo acoustic pressure wave P(r, t) can be expressed as:

$$V_{piezo}(t) = \frac{g_{33}}{A}\int_{z=0}^{t_p}\int_{A} P(r,t)\,dA\,dz$$

where, A is the area of the sensor, r is the location of the sensor surface and g_{33} is induced electric field.

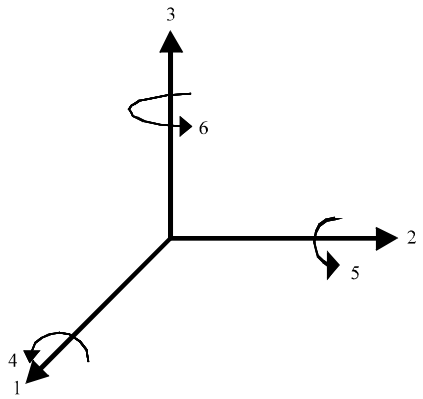

Fig. 3: Illustration of the piezoelectric constants

When the acoustic wave travels from a liquid to the piezoelectric sensor, it crosses a boundary between two materials and follows Snell's law for the angles of reflected, transmitted and refracted longitudinal and shear waves:

$$\frac{\sin\theta_{i,L}}{V_{1,L}} = \frac{\sin\theta_{r,L}}{V_{1,L}} = \frac{\sin\theta_{t,L}}{V_{2,L}} = \frac{\sin\theta_{t,S}}{V_{2,S}}$$

where, 1 is liquid, 2 is solid, θ is the angle with respect to normal to interface, i is incident, r is reflected, t is transmitted, L is longitudinal acoustic wave, S is shear acoustic wave and ν is acoustic velocity of longitudinal or shear acoustical wave.

Shear waves are generated when a longitudinal wave is incident at an oblique angle ($\grave{e}_i \neq 0°$). As in piezoelectric material the 3, 1 and 3, 2 coupling is smaller than the 3, 3 coupling, the main contribution to the piezoelectric voltage is generated by the normal component of the transmitted wave.

The 3, 1 and 3, 2 coefficients have opposite polarity, compared to the 3, 3 coefficients. This causes a decrease in voltage, when waves are incident at an increasing angle, thus reducing the opening angle of the sensor. If the generation of shear waves is neglected, the amplitude reflection and transmission coefficients R_A and T_A are given by:

$$T_A = \frac{\frac{2Z_2}{\cos\theta_t}}{\frac{Z_2}{\cos\theta_t} + \frac{Z_1}{\cos\theta_i}}; \quad R_A = \frac{\frac{Z_2}{\cos\theta_t} - \frac{Z_1}{\cos\theta_i}}{\frac{Z_2}{\cos\theta_t} + \frac{Z_1}{\cos\theta_i}}$$

where, Z is the acoustic impedance, given by:

$$Z = \frac{B}{V} = \rho v$$

where, ρ is the specific mass [kg m^{-3}], ν is the acoustic velocity [m sec^{-1}] and B is the bulk modulus [Pa]. The bulk modulus refers to the ratio of pressure to decrease in volume. If the thickness tp of the piezo is small compared to the acoustic wavelength λ_a (i.e., t_p<¼ λ_a), the integration over the thickness of the piezoelectric material can be neglected. The piezoelectric voltage can then be calculated by:

$$V_{piezo}(t) = \frac{g_{33}t_p}{A}\int_A P(r,t)T_A(r)\cos(\theta_t(r))dA$$

When the backing of the sensor is not acoustically matched with the piezoelectric material, this introduces a reflection of the acoustic wave at the piezo-backing interface. This gives an increase in the detected voltage by a factor ($1+R_A$), which in case of normal incidence on a PVdF-copper interface is equal to 1.83.

Sensor Design

The opening angle for a sensor is defined as the angle of incidence of ultrasound with respect to the normal of the sensor surface at which the amplitude of the generated voltage is decreased to half of the maximum value. To monitor local blood content in tissue, at depths up to about 3 cm, a sensor is required, which is sensitive only to variations in blood content, which occur on a line in depth. This implies that this sensor should have a very small opening angle. The shape and size of the piezoelectric element determines the characteristics of the sensor, such as the opening angle. The directional

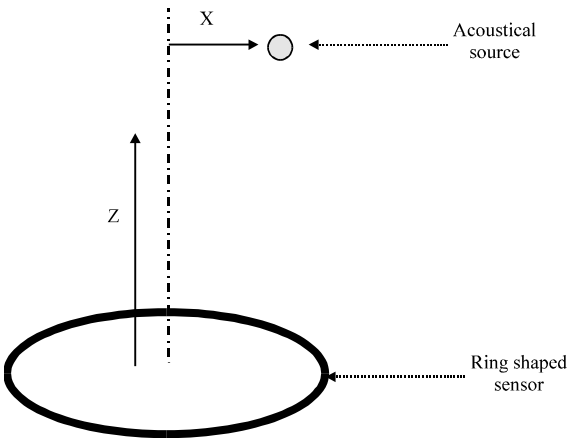

Fig. 4: Direction sensitivity and depth response

sensitivity and depth response to a spherical photo acoustic source can be calculated to characterize a sensor. The depth response is defined as the signal maximum as a function of depth of the source, while the source is located on-axis. The directional sensitivity is the signal maximum as a function of the lateral displacement of the source for a certain depth. Depth response is defined as response of the sensor to an acoustic point source located on-axis (x = 0) as a function of depth z. Directional sensitivity is defined as response of the sensor to an acoustic source located at a fixed depth z, as a function of the off-axis position x of the source. Direction sensitivity and depth response of a sensor are depicted in Fig. 4.

A spherical photo acoustic source with a Gaussian absorption distribution (1/e radius r0), homogeneously illuminated, will generate a spherical pressure wave, which at a distance r (r>>r0) from the source at time t can be described by:

$$P(r,t) = -P_{max}(r)\sqrt{e}\frac{t-\tau}{\tau_e}\exp\left\{-\frac{1}{2}\left(\frac{t-\tau}{\tau_e}\right)^2\right\}$$

$$P_{max}(r) = \frac{\beta E_a}{2\sqrt{e}(2\pi)^{3/2}C_p\tau_e^2 r};\ \tau = \frac{r}{v}$$

$$\tau_e = \sqrt{\tau_a^2+\tau_1^2};\quad \tau_a = \frac{\frac{1}{2}\sqrt{2}r_0}{v}$$

where, β is the thermal expansion co-efficient [K^{-1}], C_p is the specific heat capacity [J kg^{-1}.K], ô1 is half the pulse duration between the 1/e-points of the temporal amplitude distribution of the laser pulse [s] and Ea is the amount of laser pulse energy which is absorbed by the photo acoustic source [J].

The Sensor Width

The width of the ring is an important parameter in the design of a ring sensor. For optimal charge generation, the maximum path length difference for the acoustic signals, arriving at the ring shaped sensor, should be smaller than a quarter of the acoustic wavelength, determining the maximum width (w) of the ring shaped sensor.

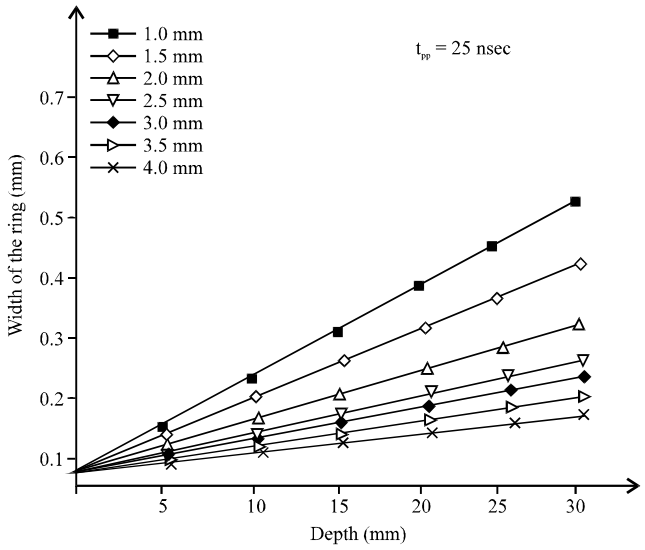

Fig. 5: A plot of the maximum width of the double ring sensor against the minimum depth at which photo acoustic signal has to be detected for peak to peak time of 25 nsec

$$\sqrt{z^2+(R+w)^2}-\sqrt{z^2+R^2}\leq \lambda/4$$

Where:

z = Depth of photo acoustic source
R = Inner radius of ring shaped sensor surface
w = Width of ring shaped sensor surface

Figure 5 gives the maximum width of the ring for various inner ring radii as a function of depth for photo acoustic sources with peak to peak times of 25 nsec. It is obvious that with increasing peak to peak time the maximum width increases. The maximum width of the ring is determined by the minimum depth at which the photo acoustic signal has to be detected with maximum charge generation. Taking an inner radius of 2.0 mm and a width of the ring of 0.17 mm, then photo acoustic signals with a peak to peak time of 67 nsec can be detected with maximum charge generation for depths larger than 7.5 mm. Besides influencing the maximum charge generation, also the width of the ring determines the broadening of the peak to peak time of the detected signals, as there will be interference of the acoustic waves, arriving at the ring shaped sensor surface. To improve the directional sensitivity of the ring-shaped sensor, two rings can be used. The effect that the directional sensitivity does not decrease very rapidly to zero can be reduced using cross-correlation techniques. Furthermore, if a side-lobe occurs in the directional sensitivity this is related to the radius of the ring.

As the second ring has a different radius, the side-lobe will appear at a different lateral displacement of the source. By simply adding the signals of both rings, the effect of side-lobes will already decrease with a factor 2.

Double Ring Sensor

Based on the described calculations of the sensor characteristics a double ring photo acoustic sensor was constructed. It consists of two concentric ring shaped sensor areas. The inner ring has an inner radius of 2 mm and a width of 0.17 mm. The outer ring has an inner radius of 3.5 mm and a width

of 0.1 mm, so that the area of both rings is equal. This sensor will be capable of detecting photo acoustic signals with a peak to peak time of 67 nsec, located at depths larger than 7.5 mm, without any significant distortion of the signals. The illumination system is integrated within the sensor module. The electrodes are constructed by using a Printed Circuit Board (PCB) with two concentric copper circles (electrodes) on it. A metal hole through the PCB connects the electrodes to the amplifiers. The piezoelectric material is glued to the PCB, using significant pressure to minimize the thickness of the glue layer. Everything is embedded in a brass housing to shield the electronics for electromagnetic noise.

With increasing depth, also signals with a smaller peak to peak time can be detected undistorted. Furthermore, for photo acoustic signals with a peak to peak time larger than 67 nsec, the minimum depth at which they are detected as being undistorted decreases further below 7.5 mm with increasing peak to peak time. In many applications of the sensor, there will be a distance between the tissue and the sensor of a few millimeters, which will be filled with ultrasound contact gel. So, the effective depth (depth in the tissue) at which the signals can be located as being undisturbed is even smaller. For application of this sensor for monitoring the blood content in the brain, the minimum depth of interest is determined by the thickness of the skin, skull and the cerebrospinal fluid layer. This total thickness is at least several milli meters. So, the limitation on the minimum depth at which the sensor can measure photo acoustic signals undisturbed will not be a problem. The depth response of the two separate rings has been calculated for a spherical photo acoustic source, which generates an acoustic signal with a peak to peak time of 67 nsec. The single sensor module has been diagrammatically shown in Fig. 6. The lateral view is shown in Fig. 7.

The sensor has been tested under different skin parameters. The perfect quantization ratio required for the skin layers and the skin densities have been maintained. Optical methods for detection of acoustic waves have been developed as well (Hoelen *et al*., 1998; Tam, 1986; Bell, 1880; Crum, 1994). But as broadband piezoelectric sensors are easier to construct and have a slightly better sensitivity than optical detection systems, the piezoelectric sensors are the best choice for this application. The maximum width of the ring is determined by the minimum depth at which the photo

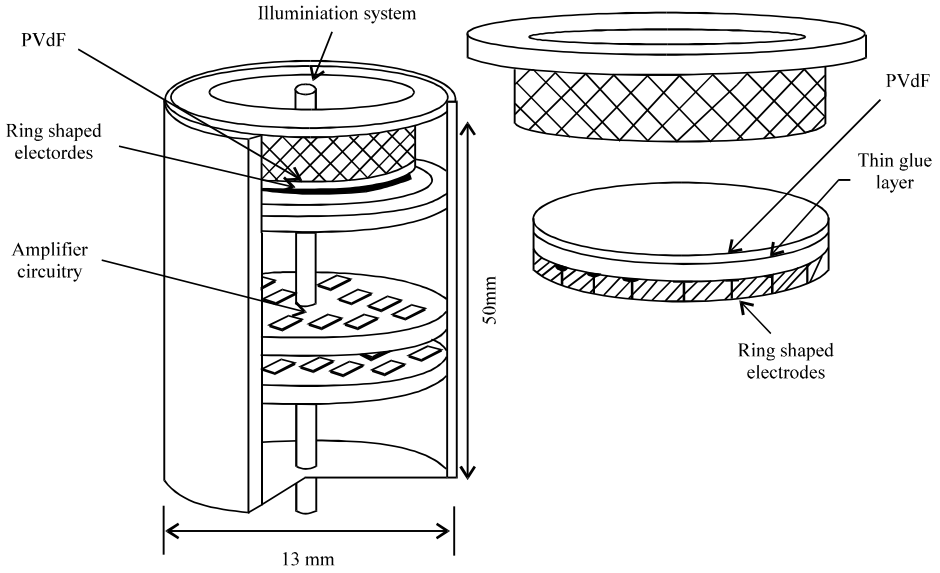

Fig. 6: The different components and layers of the double ring sensor

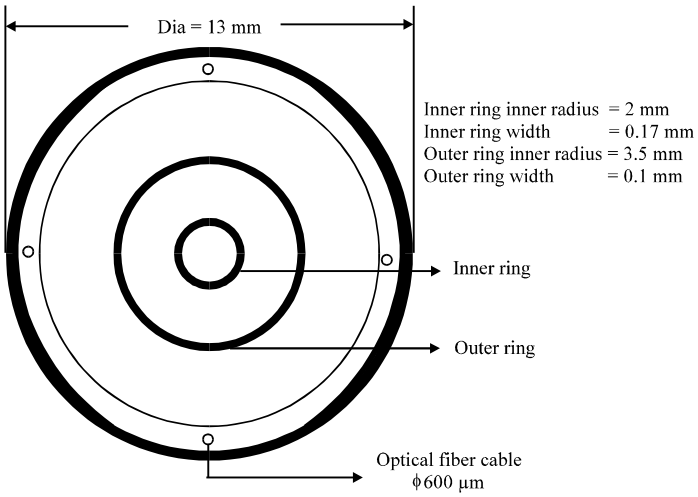

Fig. 7: Lateral view of the double ring sensor module with the ring type illumination system

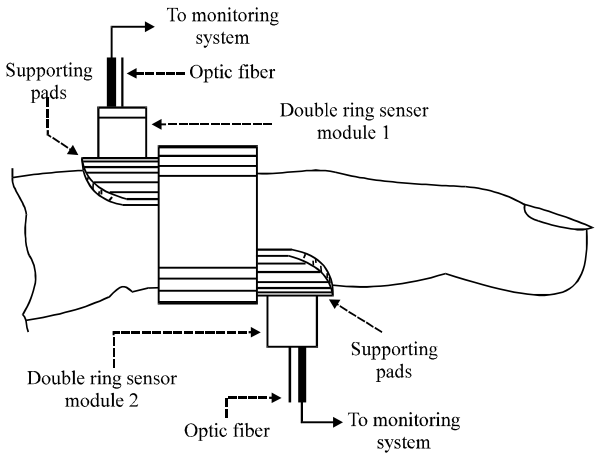

Fig. 8: Basic design for the technique in discussion

acoustic signal has to be detected with maximum charge generation. For instance, as mentioned taking an inner radius of 2.0 mm and a width of the ring of 0.17 mm, then photo acoustic signals with a peak to peak time of 67 nsec can be detected with maximum charge generation for depths larger than 7.5 mm. The model when tested with the phantom fingers brought out with maximum sensitivity. So the sensor model has been designed on a ring to fit in any one of the fingers in the real time model.

The most common piezoelectric polymer is poly vinylidene fluoride (PVDF), which is available in different thicknesses ranging from 5-100 μm as a transparent film or coated with metals for electrical contact (Sessler, 1981). In the currently used pulsed PA analysis of the blood components through the skin, the generated pressure pulses are often detected in backward mode, where excitation and detection are performed at the same side of the sample. Since piezoelectric transducers are generally not transparent, illumination through the piezo and detection at the same point are not possible. This has been overcome by using the sensor set-up shown in the Fig. 8, 9.

This PA sensor uses a transparent prism as coupling material for both illumination of the sample and transfer of the acoustic energy to the detector. The sample is eliminated through a transparent prism which also acts as an acoustic coupling material.

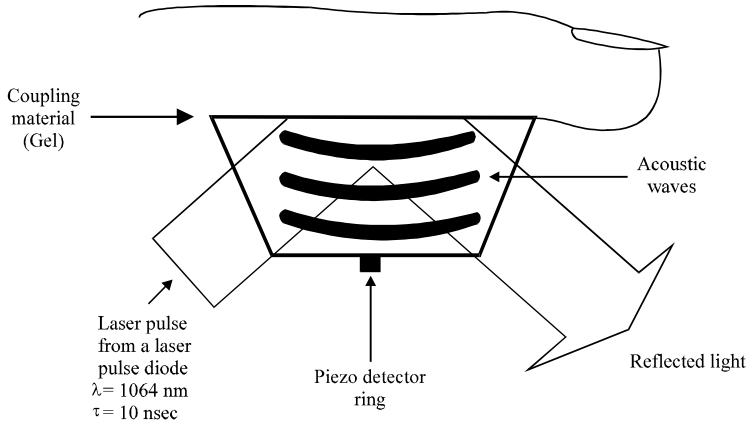

Fig. 9: Photo acoustic transduceer model

Signal Processing

In the near infrared, the scattering coefficient of the skin is much larger than its absorption coefficient. A collimated light beam at normal incident on a sufficiently thick skin can be considered. Assuming that the scattering and absorbing centers are uniformly distributed and neglecting internal light generation by fluorescence, the optical distribution can be described by the stationary radiative transfer equation, when the duration of a light pulse is longer than 10-8 nsec.

$$s.\nabla I(r,s) = -\mu eI(r,s) + (\mu e/4\pi)\int_{4\pi} p_f(s,s')I(r,s')d\omega + (\mu_e/4\pi)p_f(s,z)I_c(r,z)$$

The collimated light is attenuated according to modified Beer's law, i.e.

$$d\int c(r,z) = -\mu_e I_c(r,z).dz$$

where, Ic(r, z) is the collimated intensity at the position r in the incident direction z and r is a position vector. I(r, s) is the scattered specific intensity (watt/cm^2/sr) at the position r in the direction s and s is the directional unit vector. $P_f(s,s')$ is the phase function that represents the scattering contribution from s' in the direction s. ω' is the solid angle μ_e is the extinction coefficient defined as the sum of the absorption coefficient μ_a and the scattering coefficient μ_s.

A powerful photo acoustic technique, to be precise, the Time-Resolved Stress Detection (TRSD) can be used since it can rebuild the absorbed optical distribution by simultaneously detecting the laser induced stress amplitude. This can be used to measure the absorption and scattering coefficients together and to image the interior structure of turbid samples. Short laser pulses allow the most efficient realization of PA generation at a given incident laser fluence. Since pressure is also an important factor the PA pressure of a planar PA source produced in a clear (non- scattering) absorbing medium by a short laser pulse (δ pulse) can be described by the equation.

$$p_a(\tau) = \{E_0\alpha\beta v^2/2C_p\}\{\Theta(-\tau).\exp(\alpha v_a\tau) + R_c\,\Theta(\tau)\exp(-\alpha v_a\tau)\}$$

$$p_t(\tau_t) = \{E_0\alpha\beta v^2/2C_p\}T.\Theta(\tau_t)\exp(-\alpha v_a\tau_t)$$

Where:

$R_c = (p_t v_t - p_a v_a)/(p_t v_t + p_a v_a)$

$T = 2p_t v_t/(p_t v_t + p_a v_a)$

$\tau = t-(z/v_a)$

$\tau_t = t+(z/v_t)$

Θ is the Heaviside unit function, ρ and v are the density and the acoustic velocity of the medium, respectively. The subscripts a and t describe the parameters in the absorbing and the transparent media.

At initial time (t = 0), when the laser incidents on the absorbing medium, the above equation is simplified as:

$$P(z) = (E_0 \alpha \beta v^2 / C_p)\exp(-\alpha z) = \Gamma E_0 \alpha \exp(-\alpha z)$$

But the tissues and cells cannot be considered as non-scattering medium and hence considering the reduced scattering coefficient of the tissues μ_s' to be much larger than its absorption coefficient μ_a the corresponding stress can be modified as:

$$\begin{aligned} P(0) &= \Gamma E(0)\mu_a \qquad (z = 0)\\ P(z) &= \Gamma E_0 K_s \mu_a \exp(-\mu_{eff} z)\\ &= (1/2)\Gamma E_0 \mu_{eff} (\exp(\mu_{eff} l^*)\\ &\quad - \exp(-\mu_{eff} l^*(2\Delta + l))\}\exp(-\mu_{eff} z) \end{aligned}$$

where, $z > (1/\mu_{eff})$

For optically thick samples, $E(0) = (1+7.1R_{d\delta})\, E_0$, where $R_{d\delta?}$ is the total diffuse reflectance. $\mathbf{K}_s$ is the factor that accounts for the effect of backscattered irradiance that increases the effective energy density absorbed in the subsurface.

$$\begin{aligned} M + h\upsilon &\longrightarrow M^* + \Delta V_{el}\\ M^* &\xrightarrow{\tau} M + q\\ M^* &\xrightarrow{\tau'} + q' \xrightarrow{\tau'} P + q''\\ M^* &\longrightarrow 1 + q' + \Delta V mol\\ M^* &\longrightarrow M + q'' + h\upsilon \end{aligned}$$

Where:

$h\upsilon$	=	Energy absorbed
ΔV_{el}	=	Volumetric change
τ, τ', τ''	=	Time constants
P	=	Product after τ''
q	=	Released heat
$h\upsilon'$	=	Released energy
λ	=	1064 nm
τ	=	10 nsec

The acoustical pressure generated is:

$$P(r,t) = 1/4\pi c^* \partial/\partial t \left\{\int [P_0(r-\Delta v)/ct]ds\right\}$$

where, P (r, t) is a function of radius and time.

Also,

$$\partial^2 / \partial t^2 P(r,t) - C^2 \nabla^2 P(r,t) = \partial / \partial t \, P_0(r) \partial(t)$$

Where:

$$P_0(r) = B\beta / C_p F_0 \mu_a \exp[-z\mu_a f(x)]$$

$$\Delta r = ct$$

Where:

t = 10 nsec (from above)
c = Speed of sound 320 m sec^{-1}
C = Specific heat at constant volume
B = Bulk modulus (isothermal)

$$F(z) = F_0 \exp(-z\mu_a)$$

Where:

z = Depth
F_0 = Fluence at surface
μ_a = Absorption

RESULTS AND DISCUSSION

The real time demo model has been tested with 20 blood samples both in the diabetic range and the non diabetic range and they are satisfactory. The major implications and deductions from the output are plotted and the graphs have been illustrated here with the inferences. To assess the feasibility of photo acoustic noninvasive blood glucose detection, the technique was first used for *in vitro* studies in the mid-infrared region with aqueous glucose solutions and human whole blood (Quan *et al*., 1993). With technique in discussion, using the described measurements of the sensor (the inner ring has an inner radius of 2 mm and a width of 0.17 mm, the outer ring has an inner radius of 3.5 mm and a width of 0.1 mm) and an illumination system with a pulsed laser diode with pulse duration of 5-15 nsec and at a repetition rate of 10 Hz, the glycated hemoglobin gave a peak at 1064 nm with the peak amplitude of the photo acoustic signal varying with the glycation (number of molecules coated with glucose) of the hemoglobin.

Photo Acoustic Signal Vs. Time

The blood glucose concentration of a normal person (7% HbA1C) is previously measured with the *in vitro* techniques like the HPLC test. The analysis of the blood glucose concentration of the same person by this technique gave the output plot as shown below. The input excitation pulse for the present technique is varied for 3 wavelengths viz. 790, 960 and 1064 nm and corresponding acoustical amplitudes are together plotted (Table 2).

The peaks are shown for the different wavelength pulses in the Fig. 10. The graph gives an implication of a low peak for 1064 nm input pulse excitation which corresponds to the HbA1C. It is observed that the acoustic signals induced in the tissue start at around 2.25 μsec, representing the time of flight of acoustical waves from the arteries to the sensor surface.

Table 2: Experimental values

Time (μsec)	Distance (mm)	Photo acoustic signal strength (v) 790 (nm)	960 (nm)	1064 (nm)
0.5	0.5	0.13	0.09	0.040
0.9	0.9	0.24	0.11	0.030
1.0	1.0	0.17	0.08	0.020
1.5	1.5	-0.04	0.001	0.002
2.0	2.0	-0.01	-0.01	-0.010
2.3	2.3	0.39	0.55	0.150
3.1	3.1	-0.15	-0.26	-0.090
4.0	4.0	-0.05	-0.09	-0.001
4.8	4.8	-0.03	-0.03	-0.001

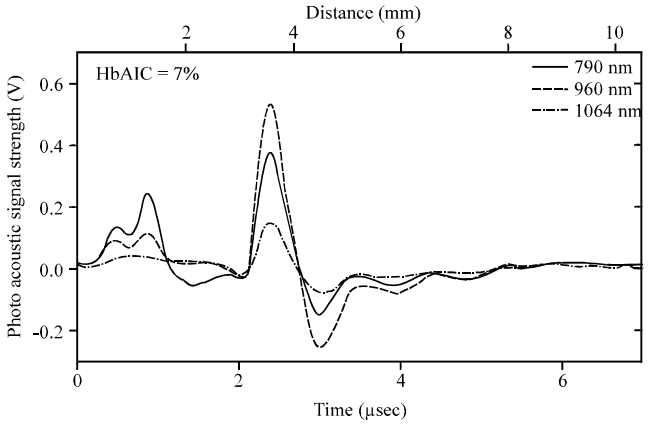

Fig. 10: A plot of PA amplitude against time for different input pulses given by a laser diode

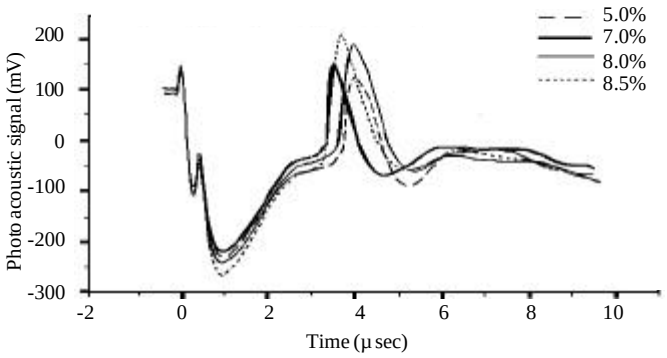

Fig. 11: Plot of photo acoustic signal Vs time for different percentages of glycated hemoglobin

The above graph is used to formulate a standard photo acoustic model of the HbA1C molecule (stable Amadori rearranged ketoamine adduct).

Variations for Different Concentrations

The plot of the acoustical signals Vs time for different concentrations of glycated hemoglobin is shown in Fig. 11. The photo acoustic signals induced in the blood start about 2-2.25 μsec. This depends on the concentration of the glucose or the glycated hemoglobin.

The first two peaks are the noise signal induced and detected by the detector system. These are not considered for any calculation purposes. Depending on the thickness of the skin there is a time

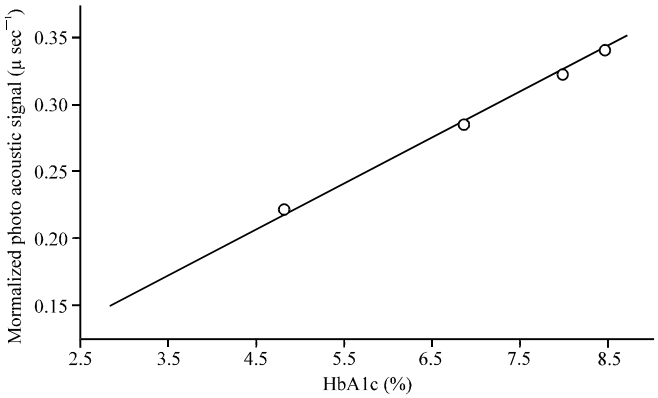

Fig. 12: Plot of normalized photo acoustic signal Vs different percentages of glycated hemoglobin

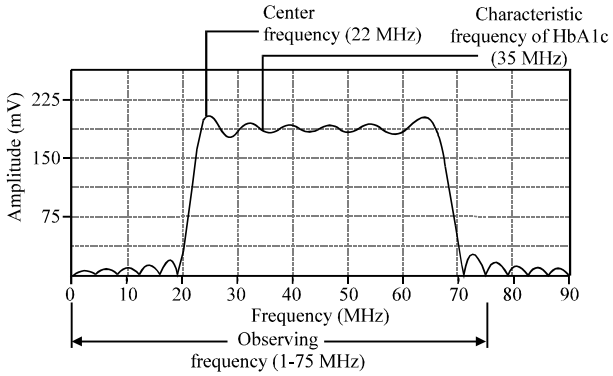

Fig. 13: Bandwidth of the filter

shift in the signals induced and this is observed in the graph plotted. The plot in Fig. 11 clearly indicates a change in the peak value with a change in the glycated hemoglobin concentration. The peak for a normal person (7%) is about 150 mV or 0.15 V. The plot is shown for four samples from among 20 patients who were tested. A 5% indicates a non-diabetic person while that greater than 7% is a diabetic patient. Once the signals are obtained the photo acoustic slope is calculated from the recorded signals and the slope is found to be linearly increasing with the glycated hemoglobin concentration. Figure 12 shows this plot.

The plot above indicates the four values of glycated hemoglobin among the 20 samples for which the testing is carried out. Before the calculation of the slope the signals are normalized. This is done in order to provide high efficiency (glycated hemoglobin % from 1-15% is clearly detected).

Frequency Analysis

As mentioned the frequency ranges from 1-75 MHz are monitored with an established center frequency at 22 MHz. The bandwidth model of the filter is shown in Fig. 13. The glycated hemoglobin frequency is estimated to be at about 35 MHz. This is the characteristic frequency output observed for the HbA1C molecule. The filters are also designed to filter out all other frequencies other that those from ±10 of the HbA1C frequency. This is then carried out for sampling and the individual signals extracted.

The pressure profile of the stress variation can also be obtained, from which various parameters including the glycated hemoglobin concentration is quantified. This is discussed in the next section.

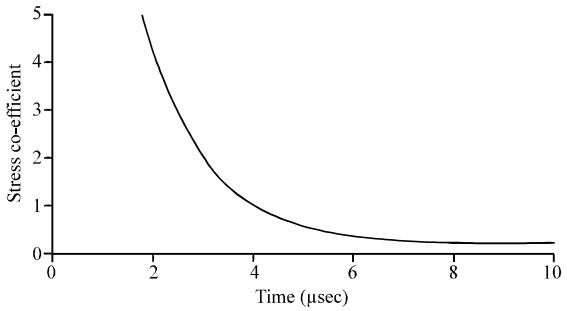

Fig. 14: Stress co-efficient Vs. time

Pressure Profile

With time resolved stress detection technique the pressure profile of the obtained photo acoustic signals is plotted using the various parameters like the stress coefficient and normalized pressure. These aspects are discussed in the following:

Stress Co-efficient Vs Time

When the stress co-efficient (in TRSD-Time Resolved Stress Detection) is plotted against the time, an exponentially decreasing curve is obtained and the following graph is plotted (Fig. 14).

The stress coefficient is an important parameter in the pressure analysis and hence has been included for discussion. It is observed from the plot that when the time t is 10 μsec, the stress co-efficient is 0.2. This attains a constant value and extends further. The plot itself begins from about 2 μsec as this is the time at which the photo acoustic signals are generated. Furthermore the stress coefficient is plotted only for the time bound range of 0-10 μsec (useful signal after 2 μsec) as the photo acoustic signals obtained within this period give the necessary information about the glycated hemoglobin concentration.

Normalized Pressure Vs Time

The second most important parameter in TRSD-Time Resolved Stress Detection is the normalized pressure. When the normalized pressure is plotted against the time, an exponentially increasing curve is obtained and the following graph is plotted (Fig. 15).

From the plot in Fig. 15, it is observed that at t = 12 μsec, the normalized pressure P_N is 0.41. The normalized acoustical pressure is found to be 0.41 at an input signal period of t_p = 10 nsec (laser pulse diode- RMI DPSS model UP-10). The plot also indicates a constant value after the 12 μsec range. Here again the plot is only for the time bound range of 2-12 μsec, the reason being the same (a useful signal between 2-12 μsec).

Determination of HbA1C Concentration from the Obtained Signals

The HbA1C concentration (%) is calculated by the various sampling processes and sorting out of the characteristic peak by analyzing the pressure profile. This is, as mentioned, dependent on the absorption coefficient of the medium (tissue, skin and blood). The absorption coefficient is used here to quantify the glycated hemoglobin. The various aspects of the absorption coefficient with the photo acoustic signals are discussed here.

Absorption Coefficient Vs HbA1C

By knowing the absorption coefficient and the molar extinction coefficient e, the glycated hemoglobin concentration is easily calculated. The absorption coefficient of the tissues and skin are related to the glycated hemoglobin concentration and these have been plotted as shown in Fig. 16.

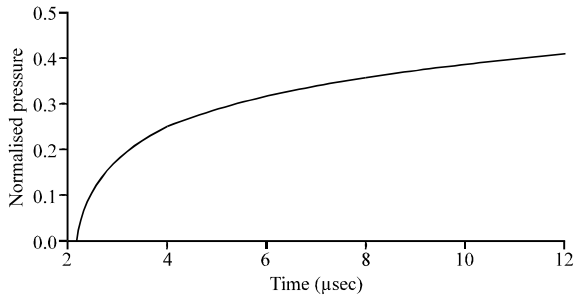

Fig. 15: Normalized pressure Vs time

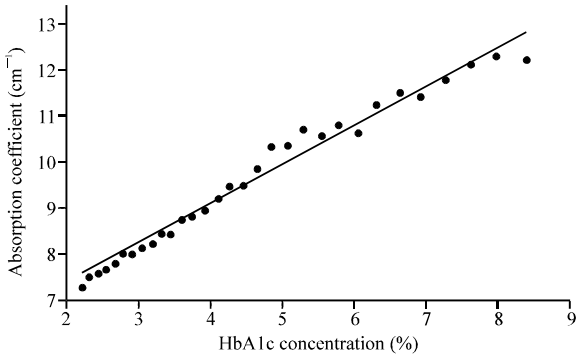

Fig. 16: Absorption coefficient Vs HbA1C

It is observed from the above plot that the variation of the hemoglobin concentration comes in a linear manner with the absorption coefficient. Though there is a slight deviation from the actual values, these results are acceptable for practical purposes.

Resultant Plot (HbA1C (%) Vs PA Signal)

Since the variation of photo acoustic signal strength with the absorption coefficient is known and the variation of the absorption coefficient with the glycated hemoglobin is also known, a correlation between the variations of photo acoustic signal strength with the glycated hemoglobin concentration is made. The resultant HbA1C concentration is thus determined from the photo acoustic output variation and when plotted on a single sheet gave the graph shown in Fig. 17.

It is observed that there is a one to one relationship between the photo acoustic signal strength and the HbA1C concentration. Though the plot is not perfectly linear, it shows a good interpretation of particular photo acoustic signal values. For example, the photo acoustic signal of strength of 0.15 V or 150 mV corresponds to glycated hemoglobin percentage of 7%.

Comparison with A Standard *in vitro* Technique

After obtaining the glycated hemoglobin percentage values through the model discussed in this work, the results are verified by comparing with a standard *in vitro* technique. The HPLC test is one of the commonly followed *in vitro* techniques for blood glucose determination. This test has been taken as the standard in this study. The following graph shows the result comparison of the above technique with the standard HPLC test (Fig. 18).

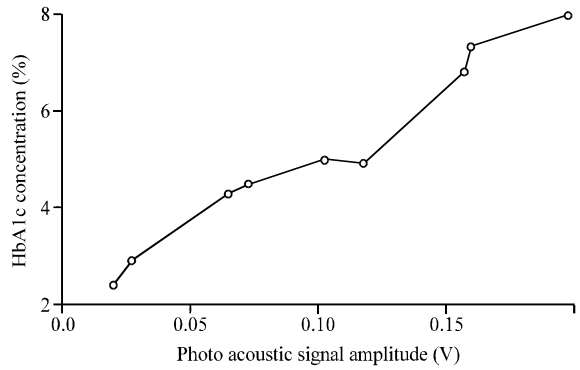

Fig. 17: Photo acoustic signals plotted against the HbA1C (%) values

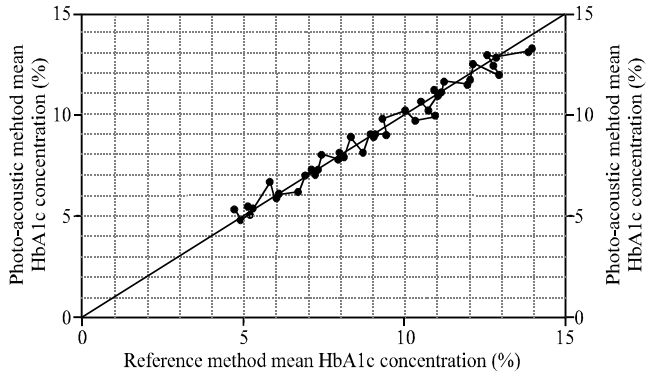

Fig. 18: Correlation between current and standard HPLC technique

It is observed from the graph that this method has only a slight variation with respect to the *in vitro* techniques and thus is very reliable. The errors and their rectification methods and other factors have been presented in the next section. The glycated hemoglobin percentage values of different patients are plotted in a comparison.

The error obtained by this technique does not stand with the Raman Spectroscopy. In Raman spectroscopy the concentration of glucose is measured directly meaning in the blood. Thus this result varies before and after food and other conditions. But this research proposes a model wherein the results shows the concentration of glycated hemoglobin which does not vary with such conditions. The measurement of glycated hemoglobin using photo acoustic technique in this research has been a novel approach, the first of its kind, in glucose quantification (glycated hemoglobin).

This technique has an error percentage of around 9%. This is observed from the graph plotted in Fig. 18. It can be made more efficient using the photo acoustic spectroscopy. The cost functions and the performance functions have been defined and stand good. The graphical results have been stated by testing the instrument under different conditions and results have been found satisfactory.

CONCLUSION

As is the need of the present scenario, this research has presented a truly non-invasive method for the glucose concentration with an acceptable error of 9%. This is a boon for the diabetics. An important facet of this method is that the test results are same in all labs. Further extended research

could lead to the measurement of the other components of blood. It can thus be concluded that this technique can be commercialized. And being a non-invasive one it would be the best among the currently available methods.

REFERENCES

Bell, A.G., 1980. On the production and reproduction of sound by light. Am. J. Sci., 20: 305-324.

Brownlee, M., A. Cerami and H. Vlassara, 1988. Advanced products of non enzymatic glycosylation and the pathogenesis of diabetic vascular disease. Diabetes Metab. Rev., 4: 437-451.

Brownlee, M., 2000. Negative consequences of glycation. Metabolism, 49: 9-13.

Crum, L.A. and R.A. Roy, 1994. Sonoluminescence. Science, 266: 233-234.

Diebold, G.J. and T. Sun, 1994. Properties of photoacoustic wave in one two and three dimensions. Acustica, 80: 339-351.

Dou, X., Y. Yamaguchi, H. Yamamoto, H. Uenoyama and Y. Ozaki, 1996. Biological applications of anti-stokes raman spectroscopy: Quantitative analysis of glucose in plasma and serum by a highly sensitive multichannel raman spectrometer. Applied Spectrosc, 50: 1301-1306.

Edward Profio, A., 1989. Light transport in tissue. Applied Opt., 28: 2216-2222.

Fischbacher, C., K.U. Jagemann, K. Danzer, U.A. Muller, L. Papenkordt and J. Schuler, 1997. Enhancing calibration models for non-invasive near-infrared spectroscopical blood glucose determination. Fresenius J. Anal. Chem., 359: 78-82.

Freeborn, S.S., J. Hannigan, F. Greig, R.A. Suttie and H.A. MacKenzie, 1998. A pulsed photo acoustic instrument for the detection of crude oil concentrations in produced water. Rev. Sci. Instrum., 69: 3948-3952.

Griffiths, P.R., 1972. Infrared emission spectroscopy. I. Basic considerations. Applied Spectrosc., 26: 73-76.

Hoelen, C.G.A., F.F.M. De Mul, R. Pongers and A. Dekker, 1998. Three dimensional photoacoustic imaging of blood vessels in tissue. Opt. Lett., 23: 648-650.

Ishimaru, A., 1989. Diffusion of light in turbid material. Applied Opt., 28: 2210-2215.

Jackson, W. and N.M. Amer, 1980. Piezoelectric photoacoustic detection: Theory and experiment. J. Applied Phys., 51: 3343-3353.

Jean-Luc Wautier, P. and J. Guillausseau, 1998. Diabetes, advanced glycation end products and vascular disease. Vascular Med., 3: 131-137.

Lane, M.D. and P.R. Christensen, 1997. Thermal infrared emission spectroscopy of anhydrous carbonates. J. Geophys. Res., 102: 25581-25592.

McCance, D.R., D.G. Dyer, J.A. Dunn, K.E. Bailie and S.R. Thorpe *et al*., 1993. Maillard reaction products and their relation to complications in insulin-dependent diabetes mellitus J. Clin. Invest., 91: 2470-2478.

Petrova, I.Y., D.S. Prough, Y.Y. Petrov, H.P.F. Brecht and C.H. Svensen *et al*., 2004. Optoacoustic technique for continuous, noninvasive measurement of total hemoglobin concentration: An *in vivo* study. Proceeding of IEEE 26th Annual International Conference on Engineering in Medicine and Biology Society, September 1-5, San Francisco, CA., pp: 2059-2061.

Quan, K.M., G.B. Christison, H.A. MacKenzie and P. Hodgson, 1993. Glucose determination by a pulsed photoacoustic technique using a gelatin based phantom. Phys. Med. Biol., 38: 1911-1922.

Seetharama Acharya, A. and J.M. Manning, 1980. Amadori rearrangement of glyceraldehyde-hemoglobin schiff base adducts. J. Biol. Chem., 255: 7218-7224.

Sessler, G.M., 1981. Piezoelectricity in polyvinylidenefluoride. J. Acoust. Soc. Am., 70: 1596-1608.

Shults, M.C., R.K. Rhodes, S.J. Updike, B.J. Gilligan and W.N. Reining, 1994. A telemetry instrumentation system for monitoring multiple subcutaneously implanted glucose sensors. IEEE Trans. Biomed. Eng., 41: 937-942.

Sternberg, F., C. Meyerhoff, F.J. Mennel, F. Bischof and E.F. Pfeiffer, 1995. Subcutaneous glucose concentration: Its real estimation and continuous monitoring. Diabetes Care, 18: 1266-1269.

Tam Andrew, C., 1986. Applications of photoacoustic sensing techniques. Rev. Mod. Phys., 58: 381-431.

Thomas Allen, J. and C. Paul Beard, 2006. Pulsed near-infrared laser diode excitation system for biomedical photo acoustic imaging. Opt. Lett., 31: 3462-3464.

Thorpe, S.R. and J.W. Baynes, 1996. Role of the Maillard reaction in diabetes mellitus and diseases of aging. Drugs Aging, 9: 69-77.

Vlassara, H., H. Fuh, Z. Makita, S. Krungkrai, A. Cerami and R. Bucala, 1992. Exogenous advanced glycosylation end products induce complex vascular dysfunction in normal animals: A model for diabetic and aging complications. Proc. Nat. Acad. Sci. USA., 89: 12043-12047.

Vlassara, H., M. Brownlee and A. Cerami, 1986. Nonenzymatic glycosylation: Role in the pathogenesis of diabetic complications. Clin. Chem., 32: B37-B41.

Wilson, E.B., J.C. Decius and P.C. Cross, 1955. Molecular Vibrations: The Theory of Infrared and Raman Vibrational Spectra. 1st Edn., McGraw-Hill, New York.